Supporting Information

A Facile, Flexible, Cost-Saving and Environment-Friendly Paper-Based Humidity Sensor for Multifunctional Applications

Zaihua Duan,[†] Yadong Jiang,[†] Mingguo Yan,[‡] Si Wang,[†] Zhen Yuan,[†] Qiuni Zhao,[†] Ping Sun,[§] Guangzhong Xie,[†] Xiaosong Du,[†] Huiling Tai*,[†]

[†]State Key Laboratory of Electronic Thin Films and Integrated Devices, School of Optoelectronic Science and Engineering, University of Electronic Science and Technology of China (UESTC), Chengdu 610054, P.R. China

[‡]College of Science, Sichuan Agriculture University, Yaan 625014, P.R. China

[§]College of Optoelectronic Engineering, Chengdu University of Information Technology, Chengdu 610225, P.R. China

Corresponding author

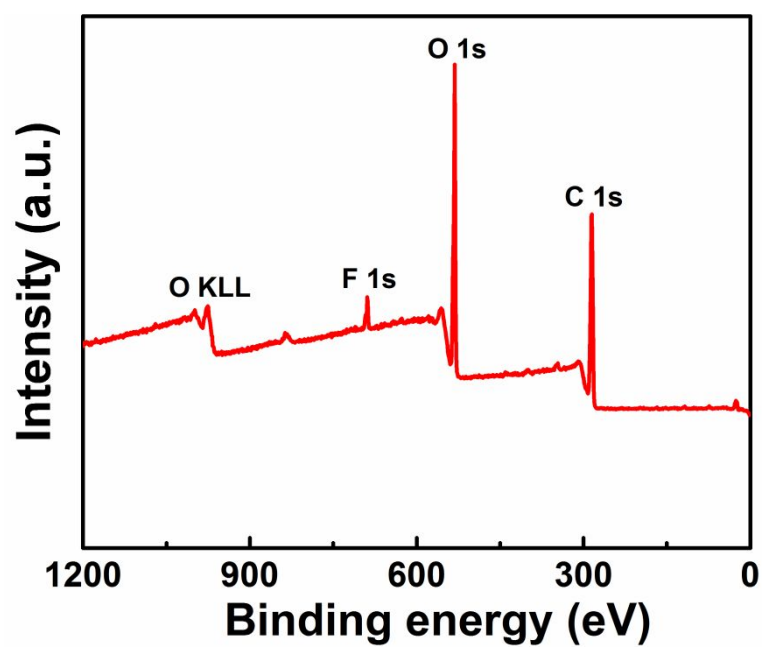*E-mail: taitai1980@uestc.edu.cn (H. T.).

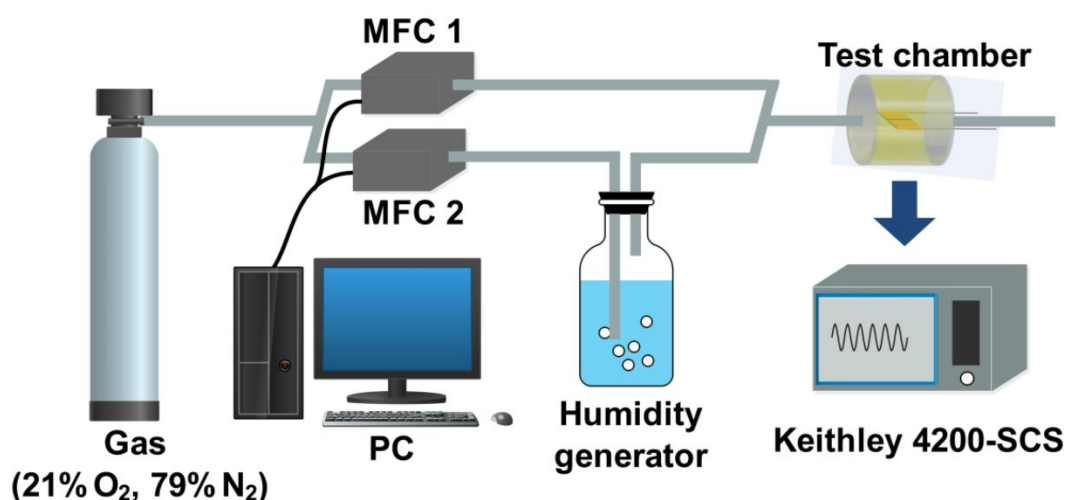**Figure S1.** XPS fully scanned spectra of the paper.

Figure S2. Schematic diagram of the humidity sensor measuring system. By bubbling dry gas in water and adjusting the mass flow ratios of dry and humidified gases, the various stable RH conditions ranging from 7.2% to 91.5% can be obtained. The total gas flow rates of two channels were precisely controlled by mass flow controllers (MFC) at a constant rate of 200 standard cubic centimeter per minute (sccm), and the flow configuration of MFC and actual measured RH by hygrometer are shown in Table S1. The volume of the test chamber is only 3 mL, so it can quickly switch different RHs. The actual RH was calibrated by a high-accuracy hygrometer (humidity accuracy: 2% RH, humidity resolution: 0.1% RH, CEM, DT-625, Shenzhen Everbest Machinery Industry Co. Ltd., China).

Table S1. **Flow Configuration of MFC and Actual Measured RH by Hygrometer.**

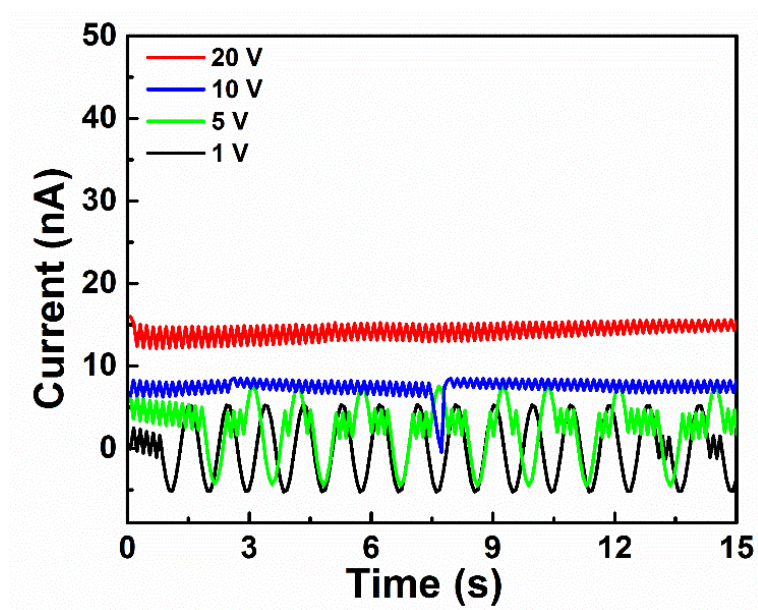| MFC 1 (sccm)	MFC 2 (sccm)	theoretical generated RH (%)	actual measured RH (%)
190	10	5	7.2
160	40	20	18.7
140	60	30	28.8
120	80	40	41.1
10	100	50	51.9
80	120	60	60.8
60	140	70	72.0
40	160	80	79.3
0	200	100	91.5

Figure S3. Output currents of the sensor under different bias voltages at 7.2% RH.

Table S2. **Comparisons on Properties of Various Paper Substrates Humidity Sensors**

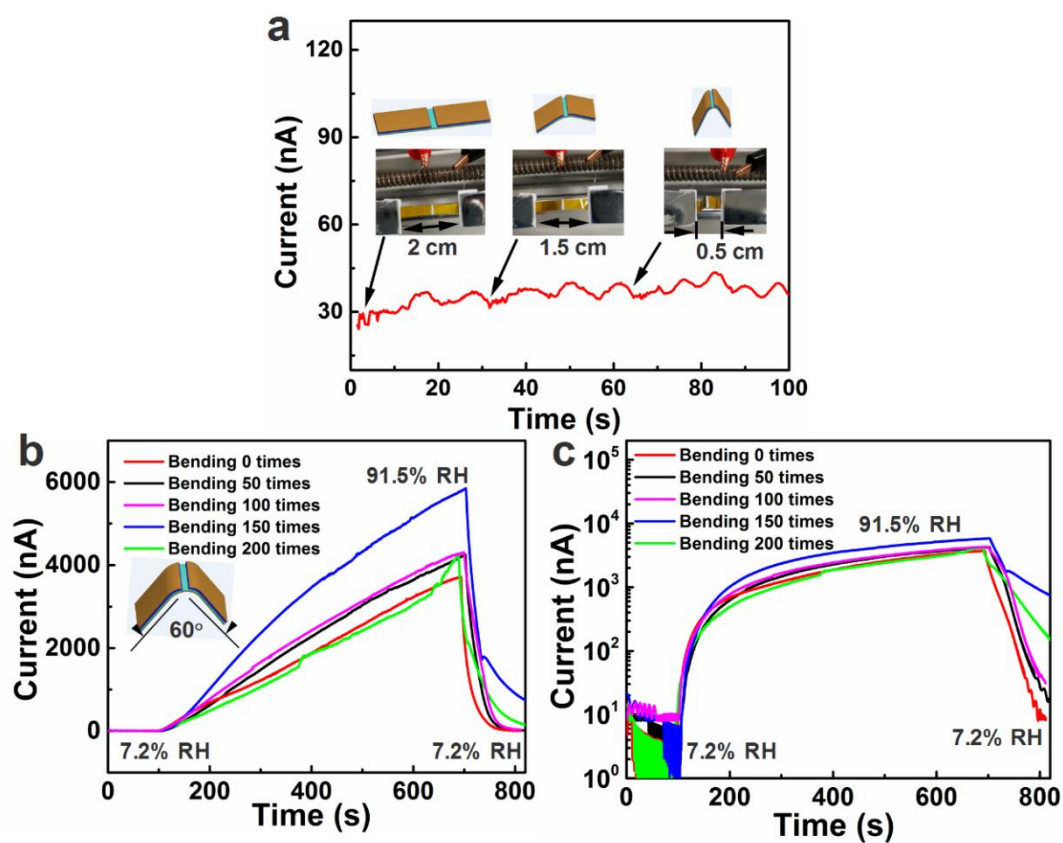| sensing	output	response	response/recovery	RH range (%)	ref.
o-MWCNTs	current	18−33% ($\Delta I/I_0$)	5−8 min/7−11 min	33−95	17
paper	frequency	~15.5% ($\Delta f/f_0$)	4 min/6 min	20−90	38
paper/graphite	voltage	215% ($\Delta V/V_0$)	~8 min/~6 min	20−70	39
PEDOT:PVMA	resistance	71−98%	−/−	11−97	40
paper	capacitance	~3.5 (C/C_0)	4 min/3 min	40−100	41
ZnO	resistance	~14 (R_0/R)	1 min/2−10 min	20−70	42
paper	current	1647 (I/I_0)	~472 s/~19 s	41.1−91.5	this work

Figure S4. (a) Real-time current curves of the humidity sensor during the bending process. Response and recovery curves in (b) linear coordinate system and (c) semi logarithmic coordinate system after different bending times of 0-200 (bending angle: 60°).
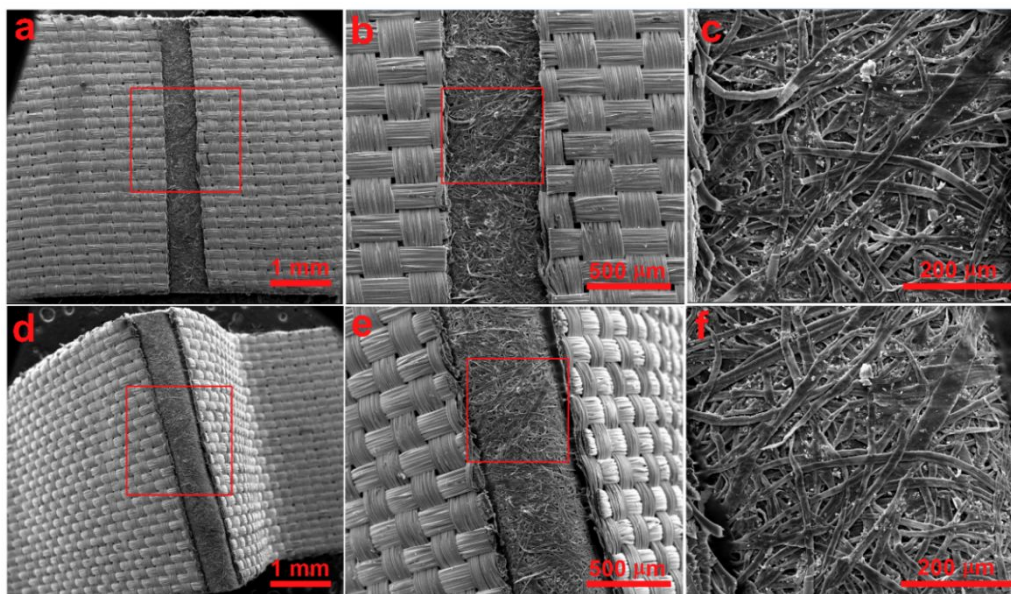
Figure S5. SEM images of the humidity sensor (a-c) before bending at flat state and (d-f) after bending 100 times at bending state.
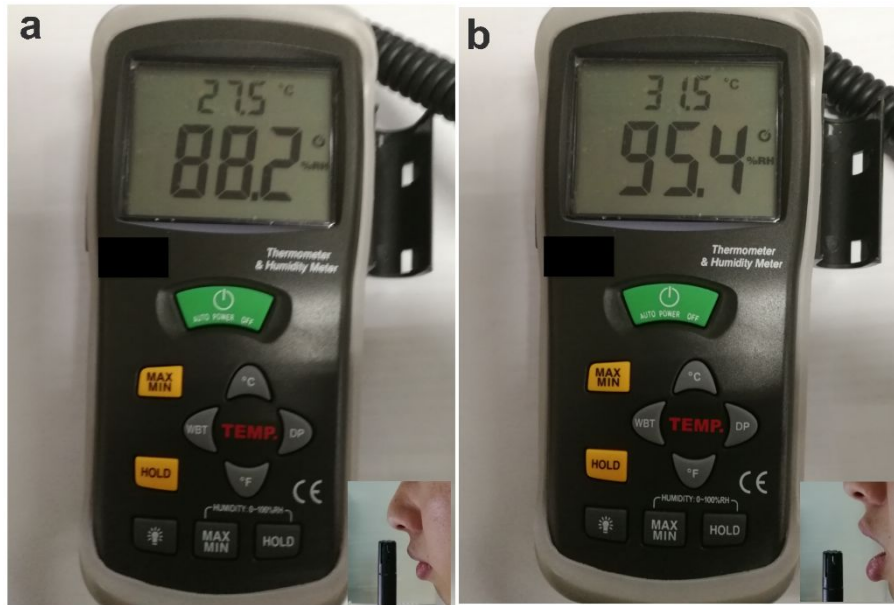
Figure S6. Actual exhaled RH of the nose (a) and mouth (b). The sensor probe of the hygrometer was placed near the nose and mouth respectively, and the nose and mouth breathing were keeping for about 30 s, respectively, until the data displayed by the hygrometer does not change. As can be seen, the RH of the breath exhaled from the mouth (95.4% RH) is higher than the nose's (88.2% RH). Because the mouth contains a lot of saliva, the RH of exhaled gas from the lungs will be close to saturated humidity (~100% RH). Although the nasal cavity is moist, it is hard to bring the RH of exhaled gas close to saturated humidity in general. In addition, the temperature of mouth breathing (31.5 °C) is higher than that of nasal breathing (27.5 °C) and the wind force of mouth breathing may be greater than that of nasal breathing, but Figure S10 proves that the humidity sensor has no noticeable responses to the changes of temperature and wind.
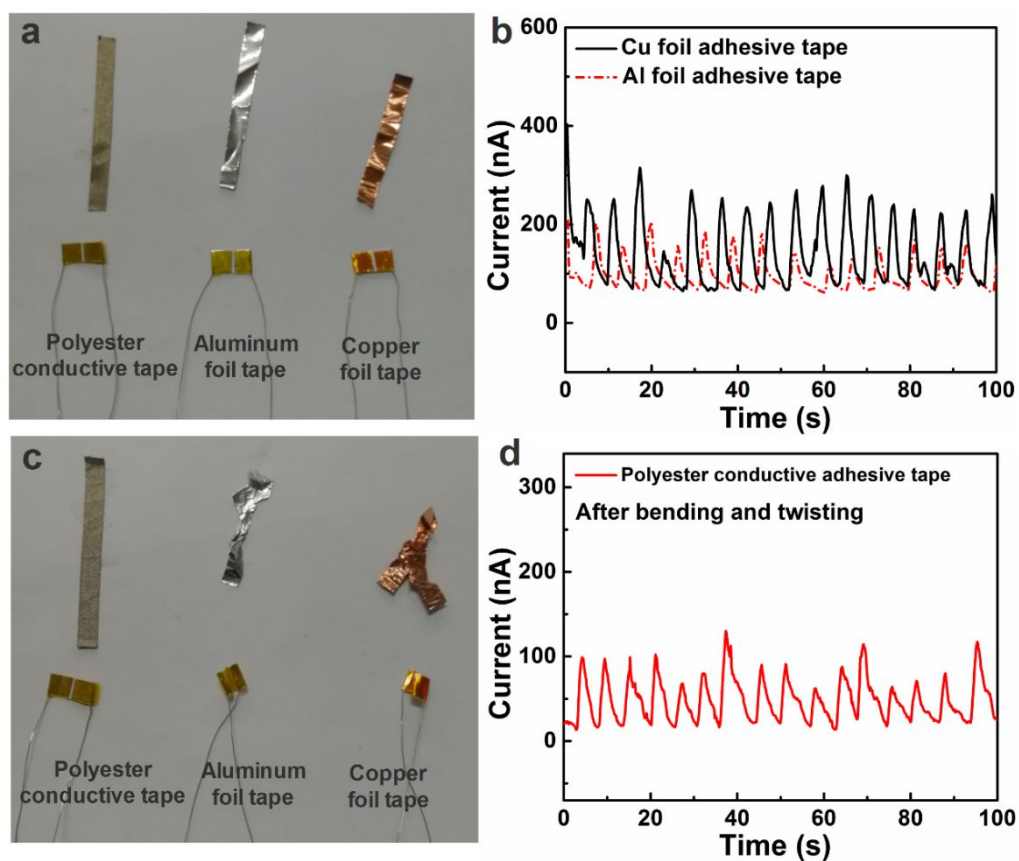
Figure S7. (a) Photograph of three electrodes materials and sensors. (b) Mouth breathing rate response curves of the humidity sensors with Cu and Al electrodes. (c) Photograph of after continuous bending and twisting the three electrodes materials and sensors. (d) Mouth breathing rate response curve of the humidity sensor with polyester electrodes after continuous bending and twisting.
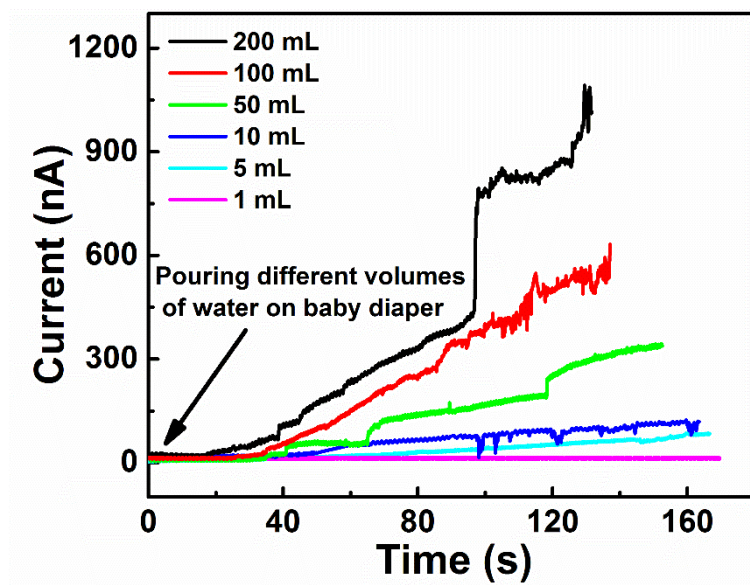
Figure S8. Real-time current curves of the humidity sensor during the baby diaper wetting process with the different volumes of water (1, 5, 10, 50, 100 and 200 mL). It should be noted that the data in Figure S8 are obtained by testing the same sensor at the different volumes of water and the distance between the position of pouring water and sensor is about 5 cm. As can be seen from the Figure S8, when the volume of water is less than 10 mL, the current of the sensor does not change significantly and the current of the sensor increases significantly when the volume of water is larger than 50 mL. This information is helpful for setting alarm threshold in the practical circuit system.
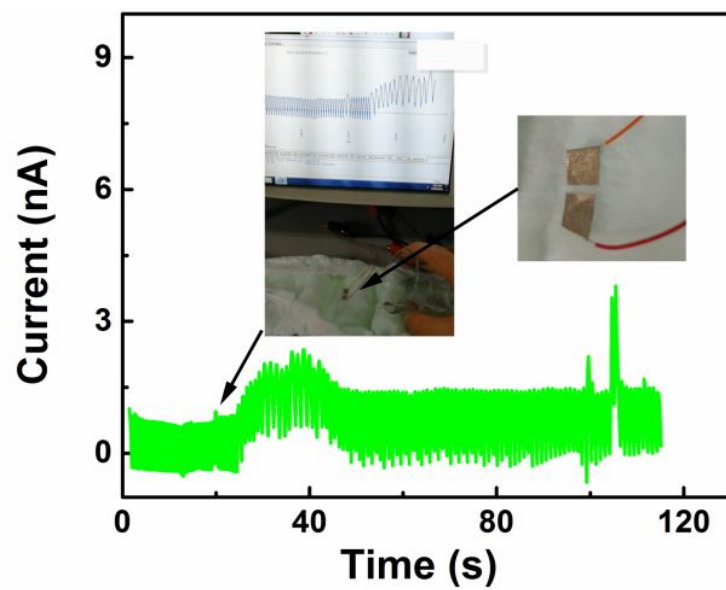
Figure S9. Real-time current curve without the paper-based humidity sensor during the baby diaper wetting process.
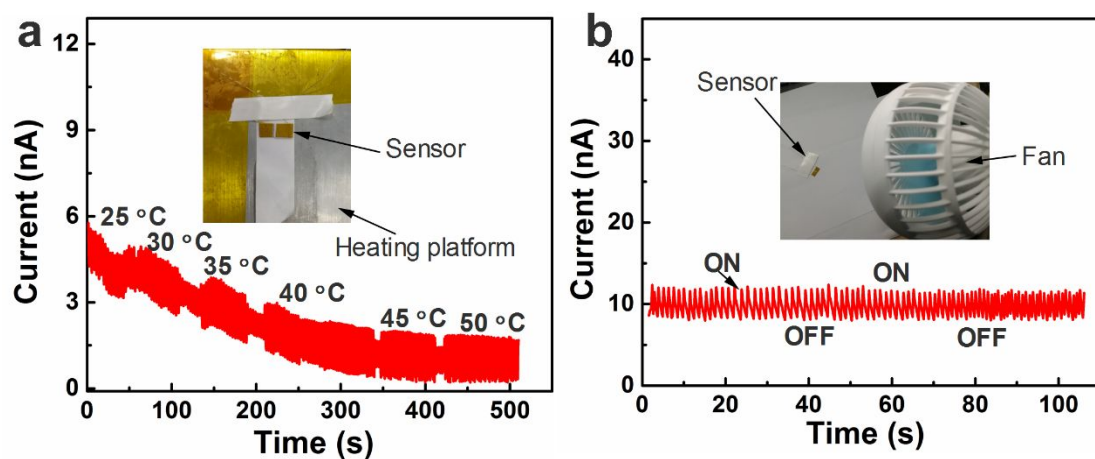
Figure S10. Responses of the humidity sensor to the changes of (a) temperature and (b) wind. As the heating temperature rises, the current of the humidity sensor decreases gradually. It can be explained that the RH around the humidity sensor decreases due to heating. Compared with the response to RH, the effect of temperature on the humidity sensing response of humidity sensor can be neglected.
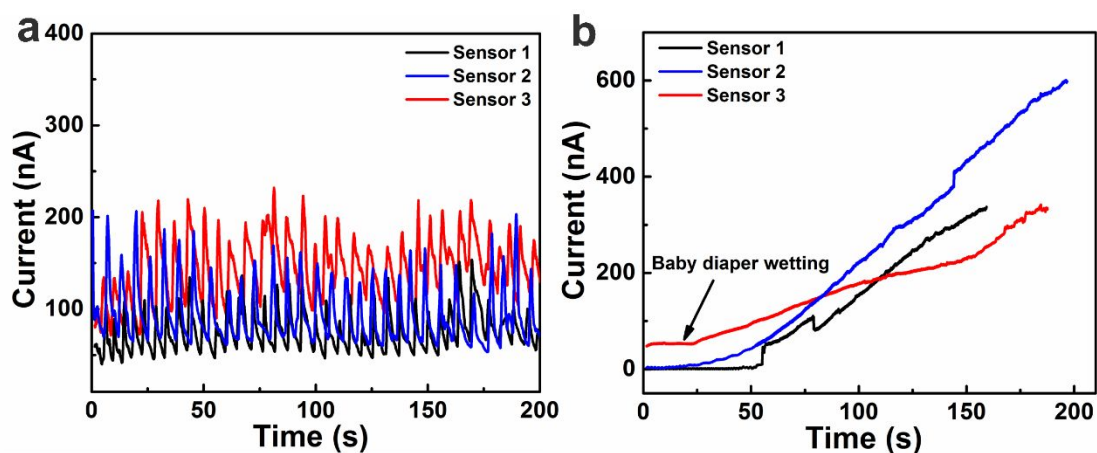
Figure S11. Consistent performance of the batch fabricated three sensors. (a) Mouth breathing rate response curves of the three humidity sensors. (b) Real-time current curves of the three humidity sensors during the baby diaper wetting process. Although the basic resistances of the three humidity sensors are not exactly the same, their responses to mouth breathing rate and baby diaper wetting are almost identical, indicating that the humidity sensors are of good consistency for detection applications.
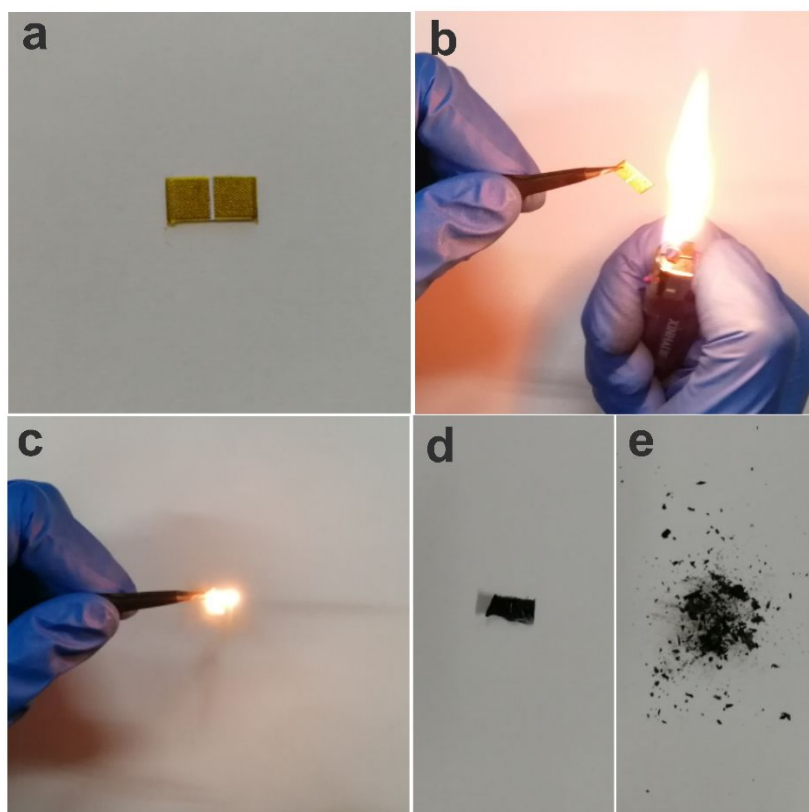
Figure S12. Photographs of disposable and degradable characteristics of the paper-based humidity sensor. (a) Before combustion, (b) ignition, (c) burning, (d) after combustion and (e) crushed ashes of the sensor. The material of the paper-based sensor is easily ignited and can be carbonized within about 3 s in air and then becomes ashes via slightly crushing.
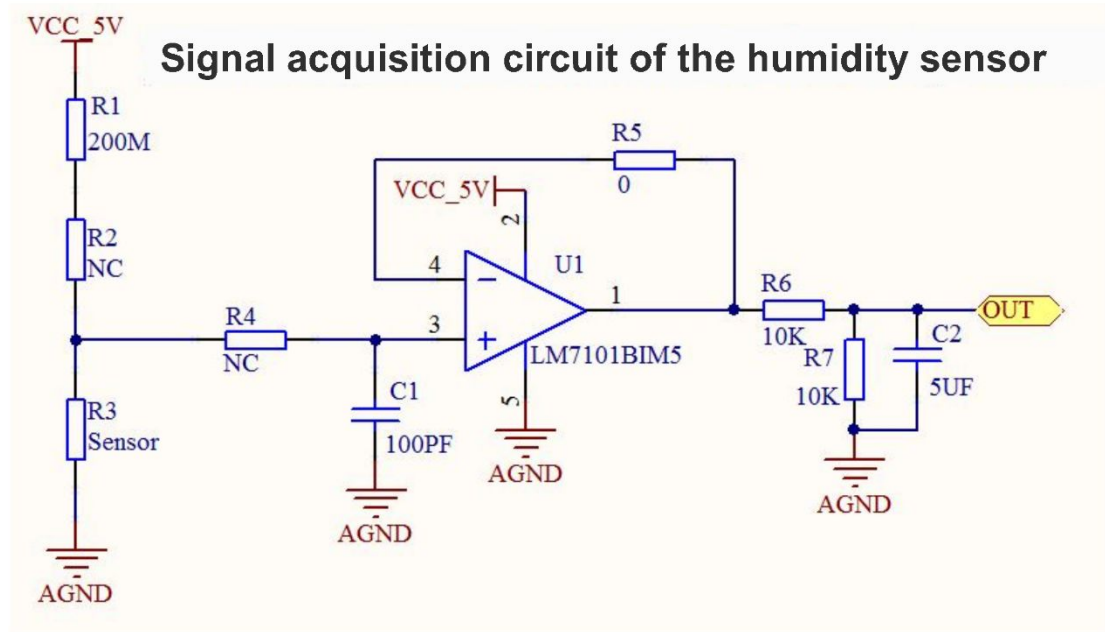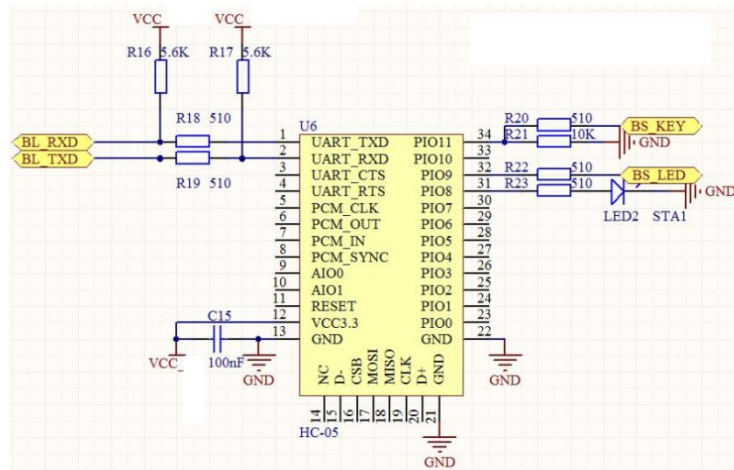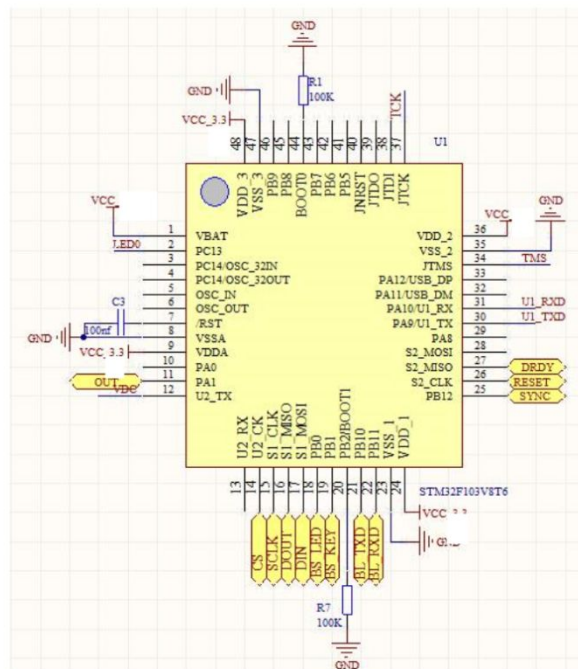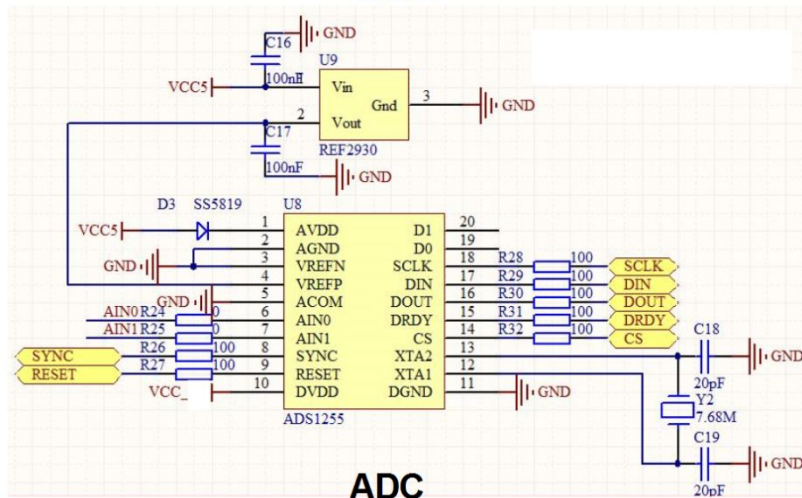
Figure S13. Schematic diagram of the data acquisition circuit. NC (No Connection) in R2, R4 is used as adjustable resistor for debugging circuit. The input impedance is very high due to the large resistance of the paper-based humidity. So, the isolation protection circuit is needed and the 0 Ω of R5 is used as a voltage follower.

Figure S14. Circuits of the bluetooth module, MCU and ADC.